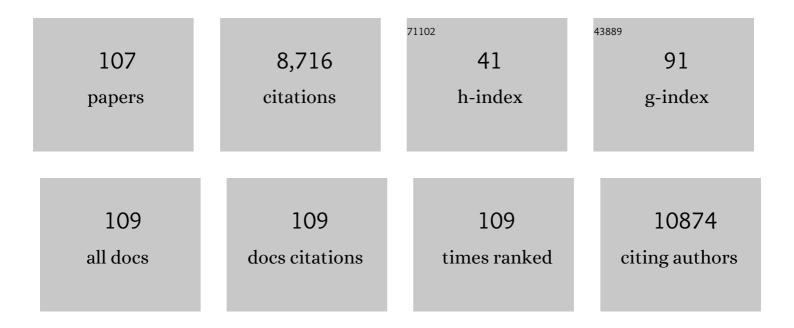
## Sungsik Lee

List of Publications by Year in descending order

Source: https://exaly.com/author-pdf/3078001/publications.pdf Version: 2024-02-01



SUNCSIE LEE

#	Article	IF	CITATIONS
1	Role of Zeolite Structural Properties toward Iodine Capture: A Head-to-head Evaluation of Framework Type and Chemical Composition. ACS Applied Materials & Interfaces, 2022, 14, 18439-18452.	8.0	27
2	Manganese Catalyzed Partial Oxidation of Light Alkanes. ACS Catalysis, 2022, 12, 5356-5370.	11.2	9
3	Silver-Loaded Xerogel Nanostructures for Iodine Capture: A Comparison of Thiolated versus Unthiolated Sorbents. ACS Applied Nano Materials, 2022, 5, 9478-9494.	5.0	10
4	Modifiers versus Channels: Creating Shapeâ€5elective Catalysis of Metal Nanoparticles/Porous Nanomaterials. Angewandte Chemie - International Edition, 2021, 60, 976-982.	13.8	30
5	Identification of engine oil-derived ash nanoparticles and ash formation process for a gasoline direct-injection engine. Environmental Pollution, 2021, 272, 116390.	7.5	6
6	Electrocatalytic Isoxazoline–Nanocarbon Metal Complexes. Journal of the American Chemical Society, 2021, 143, 10441-10453.	13.7	18
7	Single-step selective oxidation of methane to methanol in the aqueous phase on iridium-based catalysts. Applied Catalysis B: Environmental, 2021, 292, 120124.	20.2	26
8	Reaction inhomogeneity coupling with metal rearrangement triggers electrochemical degradation in lithium-rich layered cathode. Nature Communications, 2021, 12, 5370.	12.8	44
9	Facile Synthesis of Pt Carbide Nanomaterials and Their Catalytic Applications. , 2021, 3, 179-186.		8
10	Selective growth of Al2O3 on size-selected platinum clusters by atomic layer deposition. Surface Science, 2020, 691, 121485.	1.9	10
11	Site-Selective Probes of Mixed-Node Metal Organic Frameworks for Photocatalytic Hydrogen Generation. Journal of Physical Chemistry C, 2020, 124, 1405-1412.	3.1	16
12	Crystalâ€Growthâ€Dominated Fabrication of Metal–Organic Frameworks with Orderly Distributed Hierarchical Porosity. Angewandte Chemie, 2020, 132, 2478-2485.	2.0	5
13	Structural Distortion Induced by Manganese Activation in a Lithium-Rich Layered Cathode. Journal of the American Chemical Society, 2020, 142, 14966-14973.	13.7	79
14	Dynamic evolution and reversibility of single-atom Ni(II) active site in 1T-MoS2 electrocatalysts for hydrogen evolution. Nature Communications, 2020, 11, 4114.	12.8	112
15	Origins of Irreversibility in Layered NaNi <sub><i>x</i></sub> Fe <sub><i>y</i></sub> Mn <sub><i>z</i></sub> O <sub>2</sub> Cathode Materials for Sodium Ion Batteries. ACS Applied Materials & Interfaces, 2020, 12, 51397-51408.	8.0	18
16	Identification and Quantification of Technetium Species in Hanford Waste Tank AN-102. Analytical Chemistry, 2020, 92, 13961-13970.	6.5	14
17	In-situ X-ray scattering study of isotactic polypropylene/graphene nanocomposites under shear during fused deposition modeling 3D printing. Composites Science and Technology, 2020, 196, 108227.	7.8	37
18	PdCu Single Atom Alloys for the Selective Oxidation of Methanol to Methyl Formate at Low Temperatures. Topics in Catalysis, 2020, 63, 618-627.	2.8	16

#	Article	IF	CITATIONS
19	High-loading single Pt atom sites [Pt-O(OH) <i> <sub>x</sub> </i> ] catalyze the CO PROX reaction with high activity and selectivity at mild conditions. Science Advances, 2020, 6, eaba3809.	10.3	78
20	Dynamic stability of active sites in hydr(oxy)oxides for the oxygen evolution reaction. Nature Energy, 2020, 5, 222-230.	39.5	540
21	Structural reversibility of Cu doped NU-1000 MOFs under hydrogenation conditions. Journal of Chemical Physics, 2020, 152, 084703.	3.0	16
22	Unraveling the Intermediate Species of Co <sub>3</sub> O <sub>4</sub> Hollow Spheres for CO <sub>2</sub> Photoreduction by In Situ X-ray Absorption Spectroscopy. Journal of Physical Chemistry C, 2020, 124, 6215-6220.	3.1	5
23	Surpassing the single-atom catalytic activity limit through paired Pt-O-Pt ensemble built from isolated Pt1 atoms. Nature Communications, 2019, 10, 3808.	12.8	225
24	Unraveling the Origins of the "Unreactive Core―in Conversion Electrodes to Trigger High Sodium-Ion Electrochemistry. ACS Energy Letters, 2019, 4, 2007-2012.	17.4	33
25	Chemical Structure of Fe–Ni Nanoparticles for Efficient Oxygen Evolution Reaction Electrocatalysis. ACS Omega, 2019, 4, 17209-17222.	3.5	26
26	In Situ Time-Resolved X-ray Scattering Study of Isotactic Polypropylene in Additive Manufacturing. ACS Applied Materials & Interfaces, 2019, 11, 37112-37120.	8.0	39
27	Deactivation of Three-Way Catalysts Coated within Gasoline Particulate Filters by Engine-Oil-Derived Chemicals. Industrial & Engineering Chemistry Research, 2019, 58, 10724-10736.	3.7	10
28	Simultaneous in Situ X-ray Scattering and Infrared Imaging of Polymer Extrusion in Additive Manufacturing. ACS Applied Polymer Materials, 2019, 1, 1559-1567.	4.4	43
29	<i>In situ</i> , <i>operando</i> studies on the size and structure of supported Pt catalysts under supercritical conditions by simultaneous synchrotron-based X-ray techniques. Physical Chemistry Chemical Physics, 2019, 21, 11740-11747.	2.8	7
30	Low-Coordinated Pd Catalysts Supported on Zn1Zr1Ox Composite Oxides for Selective Methanol Steam Reforming. Applied Catalysis A: General, 2019, 580, 81-92.	4.3	31
31	Subnanometer cobalt oxide clusters as selective low temperature oxidative dehydrogenation catalysts. Nature Communications, 2019, 10, 954.	12.8	38
32	Controlling the 3-D morphology of Ni–Fe-based nanocatalysts for the oxygen evolution reaction. Nanoscale, 2019, 11, 8170-8184.	5.6	18
33	Single-atom gold oxo-clusters prepared in alkaline solutions catalyse the heterogeneous methanol self-coupling reactions. Nature Chemistry, 2019, 11, 1098-1105.	13.6	82
34	Coaxial Carbon Nanotube Supported TiO <sub>2</sub> @MoO <sub>2</sub> @Carbon Core–Shell Anode for Ultrafast and High-Capacity Sodium Ion Storage. ACS Nano, 2019, 13, 671-680.	14.6	41
35	Single-site Pt/La-Al2O3 stabilized by barium as an active and stable catalyst in purifying CO and C3H6 emissions. Applied Catalysis B: Environmental, 2019, 244, 327-339.	20.2	44
36	Lattice Strained Ni-Co alloy as a High-Performance Catalyst for Catalytic Dry Reforming of Methane. ACS Catalysis, 2019, 9, 2693-2700.	11.2	124

#	Article	IF	CITATIONS
37	Real-Time Visualization of Active Species in a Single-Site Metal–Organic Framework Photocatalyst. ACS Energy Letters, 2018, 3, 532-539.	17.4	69
38	NiCu single atom alloys catalyze the C H bond activation in the selective non- oxidative ethanol dehydrogenation reaction. Applied Catalysis B: Environmental, 2018, 226, 534-543.	20.2	140
39	Pt/Cu single-atom alloys as coke-resistant catalysts for efficient C–H activation. Nature Chemistry, 2018, 10, 325-332.	13.6	472
40	Dynamic Field Modulation of the Octahedral Framework in Metal Oxide Heterostructures. Advanced Materials, 2018, 30, e1804775.	21.0	13
41	Gallstone-Formation-Inspired Bimetallic Supra-nanostructures for Computed-Tomography-Image-Guided Radiation Therapy. ACS Applied Nano Materials, 2018, 1, 4602-4611.	5.0	10
42	Spectroscopic Characterization of Aqua [ <i>fac</i> -Tc(CO) <sub>3</sub> ] <sup>+</sup> Complexes at High Ionic Strength. Inorganic Chemistry, 2018, 57, 6903-6912.	4.0	10
43	Effects of Metal Composition and Ratio on Peptide-Templated Multimetallic PdPt Nanomaterials. ACS Applied Materials & Interfaces, 2017, 9, 8030-8040.	8.0	19
44	Multi-Component Fe–Ni Hydroxide Nanocatalyst for Oxygen Evolution and Methanol Oxidation Reactions under Alkaline Conditions. ACS Catalysis, 2017, 7, 365-379.	11.2	154
45	Vapor Phase Hydrogenolysis of Furanics Utilizing Reduced Cobalt Mixed Metal Oxide Catalysts. ChemCatChem, 2017, 9, 1815-1823.	3.7	14
46	Inherent Size Effects on XANES of Nanometer Metal Clusters: Size-Selected Platinum Clusters on Silica. Journal of Physical Chemistry C, 2017, 121, 361-374.	3.1	52
47	Naâ€Ion Intercalation and Charge Storage Mechanism in 2D Vanadium Carbide. Advanced Energy Materials, 2017, 7, 1700959.	19.5	168
48	Reduced Cu–Co–Al Mixed Metal Oxides for the Ring-Opening of Furfuryl Alcohol to Produce Renewable Diols. ACS Sustainable Chemistry and Engineering, 2017, 5, 8959-8969.	6.7	55
49	Mild oxidation of methane to methanol or acetic acid on supported isolated rhodium catalysts. Nature, 2017, 551, 605-608.	27.8	550
50	Mechanistic Probes of Zeolitic Imidazolate Framework for Photocatalytic Application. ACS Catalysis, 2017, 7, 8446-8453.	11.2	56
51	Dilute NiO/carbon nanofiber composites derived from metal organic framework fibers as electrode materials for supercapacitors. Chemical Engineering Journal, 2017, 307, 583-592.	12.7	66
52	Effect of Particle Size upon Pt/SiO <sub>2</sub> Catalytic Cracking of <i>n</i> â€Dodecane under Supercritical Conditions: Inâ€situ SAXS and XANES Studies. ChemCatChem, 2017, 9, 99-102.	3.7	11
53	Strongly correlated perovskite fuel cells. Nature, 2016, 534, 231-234.	27.8	387
54	Tackling CO Poisoning with Single-Atom Alloy Catalysts. Journal of the American Chemical Society, 2016, 138, 6396-6399.	13.7	374

#	Article	IF	CITATIONS
55	Combining Electronic and Geometric Effects of ZnO-Promoted Pt Nanocatalysts for Aqueous Phase Reforming of 1-Propanol. ACS Catalysis, 2016, 6, 3457-3460.	11.2	43
56	Peptide-Directed PdAu Nanoscale Surface Segregation: Toward Controlled Bimetallic Architecture for Catalytic Materials. ACS Nano, 2016, 10, 8645-8659.	14.6	58
57	Water Oxidation by Sizeâ€Selected Co <sub>27</sub> Clusters Supported on Fe <sub>2</sub> O <sub>3</sub> . ChemSusChem, 2016, 9, 3005-3011.	6.8	14
58	Fabrication of ultrafine manganese oxide-decorated carbon nanofibers for high-performance electrochemical capacitors. Electrochimica Acta, 2016, 211, 524-532.	5.2	13
59	Versatile nickel–tungsten bimetallics/carbon nanofiber catalysts for direct conversion of cellulose to ethylene glycol. Green Chemistry, 2016, 18, 3949-3955.	9.0	36
60	Facile fabrication of MnOx and N co-doped hierarchically porous carbon microspheres for high-performance supercapacitors. Electrochimica Acta, 2016, 191, 1018-1025.	5.2	13
61	Vapor phase hydrogenation of furfural over nickel mixed metal oxide catalysts derived from layered double hydroxides. Applied Catalysis A: General, 2016, 517, 187-195.	4.3	73
62	Insight into the Catalytic Mechanism of Bimetallic Platinum–Copper Core–Shell Nanostructures for Nonaqueous Oxygen Evolution Reactions. Nano Letters, 2016, 16, 781-785.	9.1	39
63	Coordination Assembly of Discoid Nanoparticles. Angewandte Chemie - International Edition, 2015, 54, 8966-8970.	13.8	25
64	Anti-P2 structured Na0.5NbO2and its negative strain effect. Energy and Environmental Science, 2015, 8, 2753-2759.	30.8	14
65	Erbium(III) Coordination at the Surface of an Aqueous Electrolyte. Journal of Physical Chemistry B, 2015, 119, 8734-8745.	2.6	14
66	Fischer–Tropsch Synthesis at a Low Pressure on Subnanometer Cobalt Oxide Clusters: The Effect of Cluster Size and Support on Activity and Selectivity. Journal of Physical Chemistry C, 2015, 119, 11210-11216.	3.1	26
67	Amine-functionalized siloxane oligomer facilitated synthesis of subnanometer colloidal Au particles. Journal of Materials Chemistry A, 2015, 3, 1743-1751.	10.3	8
68	A Common Single-Site Pt(II)–O(OH) <sub><i>x</i></sub> – Species Stabilized by Sodium on "Active―and "Inert―Supports Catalyzes the Water-Gas Shift Reaction. Journal of the American Chemical Society, 2015, 137, 3470-3473.	13.7	347
69	Identifying the Atomic-Level Effects of Metal Composition on the Structure and Catalytic Activity of Peptide-Templated Materials. ACS Nano, 2015, 9, 11968-11979.	14.6	28
70	Catalytically active Au-O(OH) <i> <sub>x</sub> </i> - species stabilized by alkali ions on zeolites and mesoporous oxides. Science, 2014, 346, 1498-1501.	12.6	544
71	Reaction Mechanism for Direct Propylene Epoxidation by Alumina-Supported Silver Aggregates: The Role of the Particle/Support Interface. ACS Catalysis, 2014, 4, 32-39.	11.2	82
72	Size- and Support-Dependent Evolution of the Oxidation State and Structure by Oxidation of Subnanometer Cobalt Clusters. Journal of Physical Chemistry A, 2014, 118, 8477-8484.	2.5	18

#	Article	IF	CITATIONS
73	Covalent heterogenization of discrete bis(8-quinolinolato)dioxomolybdenum(VI) and dioxotungsten(VI) complexes by a metal-template/metal-exchange method: Cyclooctene epoxidation catalysts with enhanced performances. Journal of Molecular Catalysis A, 2014, 392, 134-142.	4.8	3
74	Adsorbate-Induced Structural Changes in 1–3 nm Platinum Nanoparticles. Journal of the American Chemical Society, 2014, 136, 9320-9326.	13.7	69
75	In Situ Small-Angle X-ray Scattering from Pd Nanoparticles Formed by Thermal Decomposition of Organo-Pd Catalyst Precursors Dissolved in Hydrocarbons. Journal of Physical Chemistry C, 2013, 117, 22627-22635.	3.1	16
76	Spherosilicates with peripheral malonic acid and vinyl end groups. Chemical Communications, 2013, 49, 3357.	4.1	5
77	Structure Sensitivity of Oxidative Dehydrogenation of Cyclohexane over FeO <sub><i>x</i></sub> and Au/Fe <sub>3</sub> O <sub>4</sub> Nanocrystals. ACS Catalysis, 2013, 3, 529-539.	11.2	28
78	SrTiO3 Nanocuboids from a Lamellar Microemulsion. Chemistry of Materials, 2013, 25, 378-384.	6.7	38
79	Oxidation and reduction of size-selected subnanometer Pd clusters on Al2O3 surface. Journal of Chemical Physics, 2013, 138, 214304.	3.0	37
80	Controlling the Particle Size of ZrO <sub>2</sub> Nanoparticles in Hydrothermally Stable ZrO <sub>2</sub> /MWCNT Composites. Langmuir, 2012, 28, 17159-17167.	3.5	17
81	Stable Subnanometer Cobalt Oxide Clusters on Ultrananocrystalline Diamond and Alumina Supports: Oxidation State and the Origin of Sintering Resistance. Journal of Physical Chemistry C, 2012, 116, 24027-24034.	3.1	24
82	Synthesis and characterization of Au-core Ag-shell nanoparticles from unmodified apoferritin. Journal of Materials Chemistry, 2012, 22, 14458.	6.7	22
83	Supportâ€dependent Performance of Sizeâ€selected Subnanometer Cobalt Clusterâ€based Catalysts in the Dehydrogenation of Cyclohexene. ChemCatChem, 2012, 4, 1632-1637.	3.7	32
84	Shape-selective sieving layers on an oxide catalyst surface. Nature Chemistry, 2012, 4, 1030-1036.	13.6	110
85	Oxidative Dehydrogenation of Cyclohexane on Cobalt Oxide (Co <sub>3</sub> O <sub>4</sub> ) Nanoparticles: The Effect of Particle Size on Activity and Selectivity. ACS Catalysis, 2012, 2, 2409-2423.	11.2	113
86	Oxidative dehydrogenation of cyclohexene on size selected subnanometer cobalt clusters: improved catalytic performance via evolution of cluster-assembled nanostructures. Physical Chemistry Chemical Physics, 2012, 14, 9336.	2.8	38
87	Simultaneous measurement of X-ray small angle scattering, absorption and reactivity: A continuous flow catalysis reactor. Nuclear Instruments and Methods in Physics Research, Section A: Accelerators, Spectrometers, Detectors and Associated Equipment, 2011, 649, 200-203.	1.6	51
88	Size-dependent selectivity and activity of silver nanoclusters in the partial oxidation of propylene to propylene oxide and acrolein: A joint experimental and theoretical study. Catalysis Today, 2011, 160, 116-130.	4.4	115
89	Cleavage of the C–O–C bond on size-selected subnanometer cobalt catalysts and on ALD-cobalt coated nanoporous membranes. Applied Catalysis A: General, 2011, 393, 29-35.	4.3	24
90	Communication: Suppression of sintering of size-selected Pd clusters under realistic reaction conditions for catalysis. Journal of Chemical Physics, 2011, 134, 141101.	3.0	25

#	Article	IF	CITATIONS
91	Oxidative Decomposition of Methanol on Subnanometer Palladium Clusters: The Effect of Catalyst Size and Support Composition. Journal of Physical Chemistry C, 2010, 114, 10342-10348.	3.1	76
92	Catalysis by Supported Size-Selected Clusters. , 2010, , 345-365.		2
93	Increased Silver Activity for Direct Propylene Epoxidation via Subnanometer Size Effects. Science, 2010, 328, 224-228.	12.6	783
94	Combined TPRx, in situ GISAXS and GIXAS studies of model semiconductor-supported platinum catalysts in the hydrogenation of ethene. Physical Chemistry Chemical Physics, 2010, 12, 5585.	2.8	37
95	Selective Propene Epoxidation on Immobilized Au <sub>6–10</sub> Clusters: The Effect of Hydrogen and Water on Activity and Selectivity. Angewandte Chemie - International Edition, 2009, 48, 1467-1471.	13.8	246
96	Combined temperature-programmed reaction and <i>in situ</i> x-ray scattering studies of size-selected silver clusters under realistic reaction conditions in the epoxidation of propene. Journal of Chemical Physics, 2009, 131, 121104.	3.0	41
97	Growth of Metal Oxide Nanowires from Supercooled Liquid Nanodroplets. Nano Letters, 2009, 9, 4138-4146.	9.1	70
98	A study of the electronic structure and reactivity of V/TiO2(110) with metastable impact electron spectroscopy (MIES) and ultraviolet photoelectron spectroscopy (UPS). Topics in Catalysis, 2006, 38, 127-132.	2.8	13
99	Agglomeration, Sputtering, and Carbon Monoxide Adsorption Behavior for Au/Al2O3Prepared by Aun+Deposition on Al2O3/NiAl(110). Journal of Physical Chemistry B, 2005, 109, 11340-11347.	2.6	38
100	Agglomeration, support effects, and CO adsorption on Au/TiO2(110) prepared by ion beam deposition. Surface Science, 2005, 578, 5-19.	1.9	92
101	Cluster size effects on CO oxidation activity, adsorbate affinity, and temporal behavior of model Aunâ^•TiO2 catalysts. Journal of Chemical Physics, 2005, 123, 124710.	3.0	87
102	Hydrazine Decomposition over Irn/Al2O3Model Catalysts Prepared by Size-Selected Cluster Deposition. Journal of Physical Chemistry B, 2005, 109, 381-388.	2.6	36
103	CO Oxidation on Aun/TiO2Catalysts Produced by Size-Selected Cluster Deposition. Journal of the American Chemical Society, 2004, 126, 5682-5683.	13.7	338
104	Deposition dynamics and chemical properties of size-selected Ir clusters on TiO2. Surface Science, 2003, 542, 253-275.	1.9	62
105	Sintering, oxidation, and chemical properties of size-selected nickel clusters on TiO2(110). Journal of Chemical Physics, 2002, 117, 5001-5011.	3.0	48
106	Cu wetting and interfacial stability on clean and nitrided tungsten surfaces. Applied Surface Science, 2001, 171, 275-282.	6.1	19
107	Single-Atom Metal Oxide Sites as Traps for Charge Separation in the Zirconium-Based Metal–Organic Framework NDC–NU-1000. Energy & Fuels, 0, , .	5.1	8